On-Demand Metal-to-Metal Electron Donation During Zr-Ru Heterodinuclear Catalyzed Amine-Borane Dehydrogenation

Jugal Kumawat and Daniel H. Ess*
Department of Chemistry and Biochemistry, Brigham Young University, Provo 84604, Utah, United States

Abstract

Dinuclear metal-metal cooperative effects are important in catalysis involving the activation of small molecules with strong bonds. Here we report density functional theory calculations used to determine the catalytic mechanism and metal-metal cooperative effects during amine-borane dehydrogenation catalyzed by a Zr-Ru heterodinuclear complex. These calculations revealed that during catalysis bond activation steps occur mainly at the Zr center and the Ru metal plays a role as a ligand-like on-demand electron donation partner. We also used calculations to determine the mechanistic and reactivity difference between the dinuclear Zr-Ru complex and mononuclear Zr and Ru complexes.

Introduction

A metal-metal interaction[1,2,3,4,5,6] in heterodinuclear complexes has the potential to induce unique mechanisms and reactivity during catalysis.[7,8,9,10,11,12,13,14,15] Dinuclear metal-metal cooperative effects are particularly important to exploit in catalysis where there are difficult small molecule bond activation reaction steps. As an example, Lau and co-workers[16] reported a heterodinuclear Ru-Mn complex that catalyzes activation of carbon dioxide to induce coupling with an epoxide to form carbonates. Thomas and coworkers have synthesized a series of Co-Zr complexes for N–H bond activation of hydrazines,[17] CO_2 activation,[18,19] and activation of carbon-heteroatom bonds.[20] In more recent examples, Nakao reported Rh-Al complexes for C−O/C−C/C−F bond activation[21,22,23] and Takaya and Iwasawa reported a Pd-Al complex for hydrosilylation of CO_2.[24]

Amine-borane dehydrogenation requires the activation of strong N–H and B–H bonds, and because of the umpolung polarity of these two different bonds this reaction is potentially susceptible to metal-metal cooperative effects.[25,26,27,28,29,30,31,32,33,34,35,36] This reaction is important because of its potential for chemical hydrogen storage,[25,26,37,38] regeneration of spent fuel,[39,40,41] and creation of B−N-polymeric materials.[25,42,43] Manners and coworkers[25,28,29,30,31,32,33,34] have developed a series of different metal-metal and metal-ligand based complexes for dehydrogenation of N-methylamine-borane and ammonia-borane. Related, Peters and coworkers have reported a Co-boryl complex for amine−borane dehydrogenation to hydrogenate olefins.[35]

Our computational work here focuses on Nishibayashi and coworker's[36] report of a Zr-Ru heterodinuclear complex **1** featuring a metallocenyl diphosphine bridging ligand that catalyzes amine-borane dehydrogenation (Scheme 1a and1b). We became interested in the details of this reaction because it was unclear how the metal-metal interaction influences catalysis. For example, are both metal centers involved in bonding changes or does one metal dominate catalysis and the other metal act as a fixed center? Therefore, we used density functional theory (DFT) calculations to evaluate the catalytic mechanism and the metal-metal cooperative effect for Zr-Ru catalysis of amine-borane dehydrogenation. These calculations revealed that bond activation steps (e.g. N–H activation) occur mainly at the Zr center and the Ru metal plays a role as an on-demand electron donation partner (Scheme 1c). Transition states show a continuum from full or partial Ru-to-Zr

donation to no donation with a completely severed Zr-Ru interaction. We also used calculations to determine the mechanistic and reactivity difference between the Zr-Ru complex and mononuclear Zr and Ru complexes, which is important in evaluating the advantage of heterodinuclear catalysts. Nishibayashi and coworkers reported that the Zr-Ru complex provides >90% H_2 conversion whereas a related mononuclear Ru complex provides less than 20% conversion.[36] Perhaps surprisingly, calculations show that while the analogous mononuclear Ru complex indeed has much higher barriers for amine-borane dehydrogenation simple model mononuclear Zr complexes have comparable barriers. This suggests that one major advantage of the Zr-Ru heterodinuclear catalyst is not turnover reactivity but rather stability and ease of precatalyst to catalyst transformation.

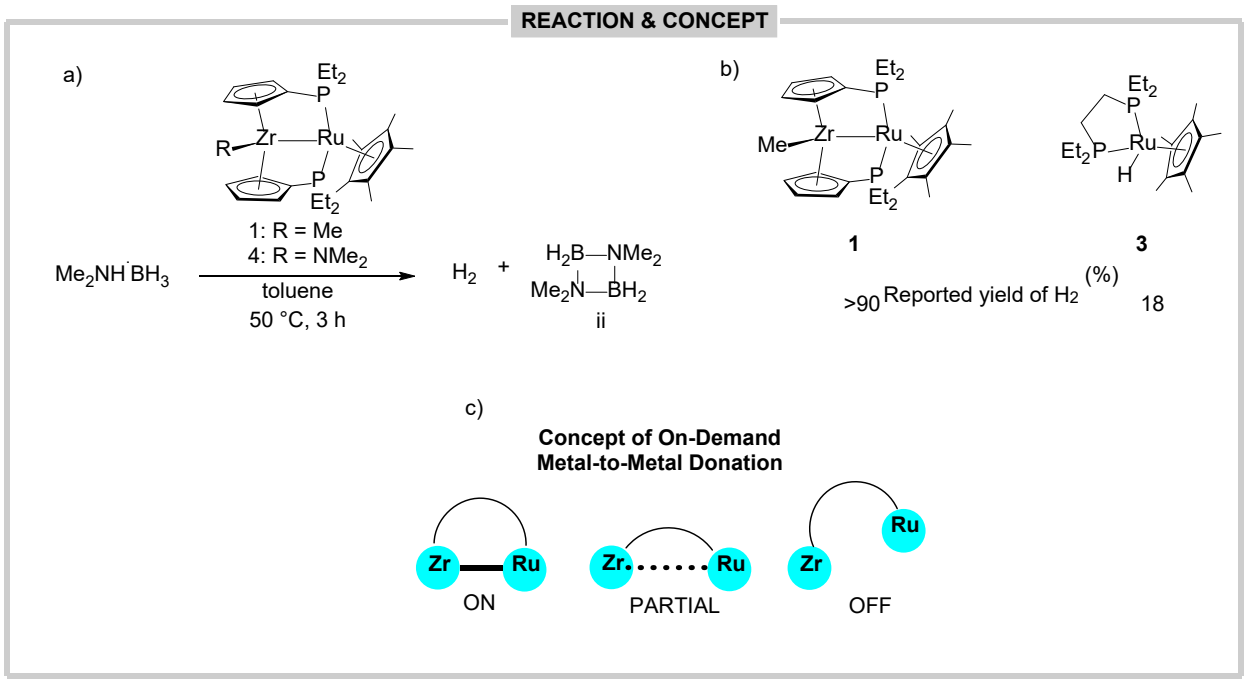

Scheme 1. a) Amine-borane dehydrogenation reaction catalyzed by Zr-Ru heterodinuclear complex **1** reported by Nishibayashi.[36] b) Comparison of heterodinuclear and mononuclear catalysis by H_2 conversion yields reported by Nishibayashi.[36] c) Highlight of the on-demand metal-to-metal donation effect that was discovered in this work.

Results and Discussion

Scheme 2 provides a general catalytic cycle for $Me_2NH{\cdot}BH_3$ (**i**) dehydrogenation by precatalyst complexes **1** and **4**, which was originally outlined by Nishibayashi.[36] Entry into the cycle begins with generation of the Zr–H intermediate **1c** (proposed as a bridged hydride between the Zr and Ru centers) that then facilitates N–H activation to generate a Zr–H/Ru–H intermediate **1g**. Subsequent reductive elimination to form H_2 gives the Zr-amine intermediate **1h** with a proposed reformed metal-metal interaction. B–H bond activation then reforms the Zr–H intermediate.

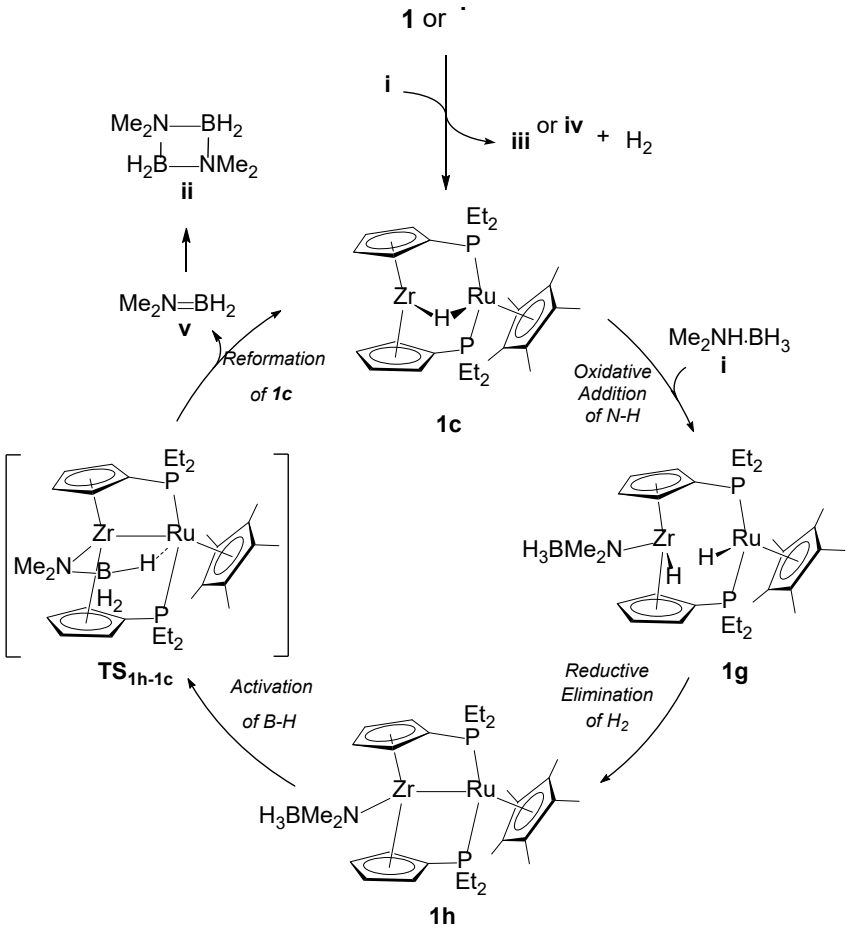

Scheme 2. General mechanism for amine-borane dehydrogenation with the Zr-Ru heterodinuclear catalysis that was originally proposed by Nishibayashi.[36]

With the precatalyst having a proposed Zr-Ru interaction and then during the catalytic cycle the interaction being potentially broken and reformed we started with a natural bond orbital analysis of the metal-metal bonding in **1**. Figure 1a displays the natural bond orbitals for **1**. For **1**, as expected, there are three nonbonding d-orbitals centered on Ru (HOMO-5, HOMO-6 and HOMO-7). The Zr−Ru interaction is best described by the HOMO orbital and is comprised of 35% contribution from Zr and 65% from Ru suggesting a polar covalent bond. For a frame of reference, the Zr-CH_3 bond in **1** has 23% contribution from Zr and 77% contribution from the carbon. Based on this orbital analysis, perhaps the best metal oxidation assignments for Zr and Ru are +3 and +1, respectively. We also examined the structure and orbitals of **1c**. In contrast to the proposed structure shown in Scheme 2, the non-bridged structure with an intact Zr−Ru bond is significantly (30.0 kcal/mol) lower in energy than the bridged structure (Figure 1b). The orbital bonding of **1c** is very similar to **1**, and for the Zr−H bond in **1c** is comprised of 37% from Zr and 63% from H.

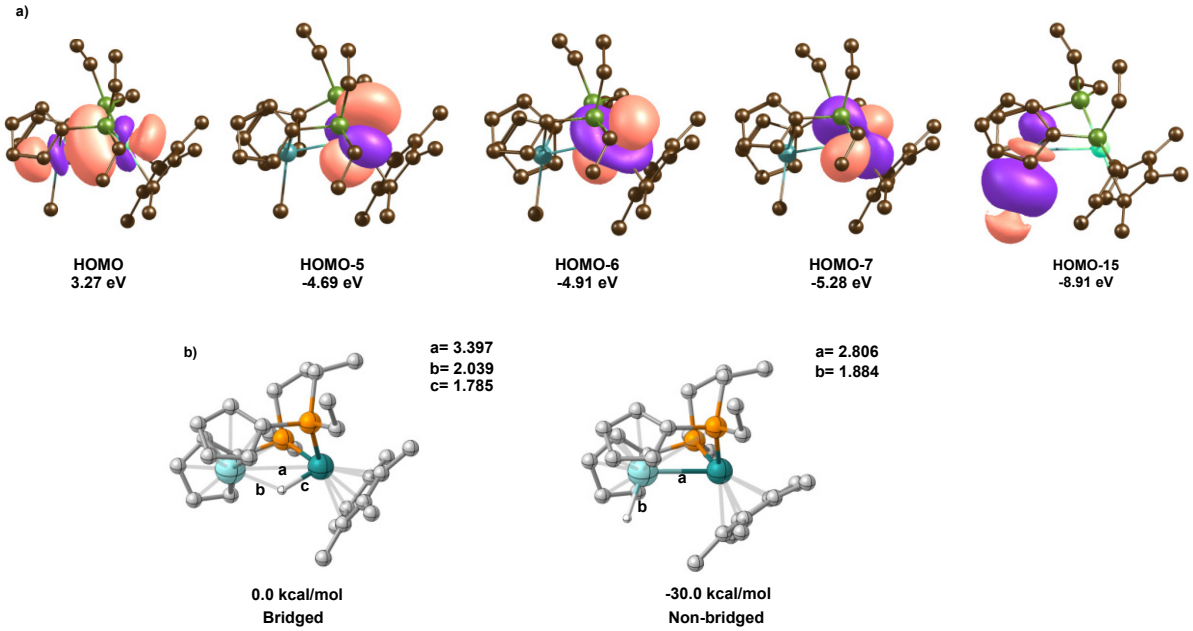

Figure 1. a) B3LYP natural bond orbitals for complex **1**. b) 3D structure comparison of bridged and non-bridged versions of **1c**. Hydrogens have been removed for visual clarity.

For amine borane (and ammonia borane) there have been a variety of dehydrogenation mechanisms proposed, especially for mononuclear and organic catalysis. These mechanisms have been reviewed by Paul.[44] Generally, mononuclear mechanisms can be categorized as either metal centered where all the coordination and bond making and breaking occurs at the metal center or metal-ligand cooperative where the ligand also assists in bond making and breaking. Additionally, in both of these categories there is also the possibility of concerted mechanisms where both the B–H and N–H bonds are broken in the same reaction step or stepwise mechanisms where there is first one bond broken and then the other. Generally stepwise mechanisms occur in a polar fashion with a proton that comes from the N–H bond and a hydride that comes from the B–H bond. In addition to these general categories there are also unique mechanisms that have been proposed, such as S_E2 mechanism where the metal induces ammonia transfer and dislodges borane.[45] Also, perhaps due to the polarity of the N–H and B–H bonds (compared to less polar C–H bonds) many of the reaction steps proposed and transition states located with calculations only partially resemble traditional organometallic type reaction steps, such as metal insertion/oxidative addition and β-hydride elimination.

As an example of a metal centered mechanism, Paul and Musgrave showed with DFT calculations that with a mononuclear Ir pincer catalyst the reaction likely proceeds through a mechanism with metal centered concerted removal of hydrogen.[46,47,48,49] For the related Fe pincer catalyst a concerted mechanism using both the metal center and ligand was proposed.[50] Macgregor and Weller using both DFT calculations and experiment showed that for a cationic Ir pincer complex the dehydrogenation also occurs through a metal centered mechanism.[51] In contrast to the concerted metal centered mechanism proposed by Paul and Musgrave, Luo and Ohno based on DFT calculations proposed a stepwise reaction mechanism for amine borane dehydrogenation by a titanocene catalyst.[52,53] In this reaction the Ti metal center induces N–H bond activation/oxidative addition first step to generate a Ti–H amine intermediate followed by a second

step of hydride abstraction from the boron. Somewhat related stepwise pathways have been proposed by Esteruelas,[54] Kawano and Shimoi,[55] Conejero,[56] and Schneider.[57]

There have been a variety of metal-ligand cooperative mechanisms proposed. For example, Hall used DFT calculations to examine ammonia borane dehydrogenation by a mononuclear Ni(NHC) catalyst and found that part of the reaction mechanism involves proton transfer to the NHC ligand followed by Ni induced C-H activation.[58,59,60,61] A related mechanism has also been proposed for a Pd(NHC) catalyst.[62,63] However, it has been proposed that free NHC might also catalytically induce dehydrogenation.[64] It is useful to note that in many of the calculated mechanisms there are generally proposed coordination[65] of B–H and N–H bonds prior to bond activation. Some of these coordination modes have been experimentally observed by Weller[66,67,68,69] and Sabo-Etienne.[70]

For Zr-Ru complexes **1** and **4** in addition to possible metal centered and metal-ligand mechanisms there is also the possibility of metal-metal cooperative mechanisms. Therefore, all three of these general types of mechanisms (both concerted and stepwise) were explored for both precatalyst to active catalyst conversion as well as for every step of the substrate to product conversion. To begin, we examined possible pathways that most directly generate compound **iii**, which was observed experimentally, where the methyl group is transferred to the borane with formation of the Zr–H. Alternatively, the Zr–H intermediate **1c** can be generated while also forming methane, but there was no report of methane being experimentally detected. See the Supporting Information (SI) discussion about this pathway, which involves a formal σ-bond metathesis between the Zr–Me and the amine borane N–H bond. Figure 2 shows the Gibbs energy reaction coordinate landscape for the formation of **1c** from **1**. Initially $Me_2NH{\cdot}BH_3$ **i** coordinates to **1** through the borane B–H bond and **1a** is endergonic by 4.9 kcal/mol. This endergonic intermediate can then undergo a four-centered σ-bond metathesis transition state (**$TS_{1a\text{-}1b}$**) where the boron delivers a hydride and abstracts a methyl group from the Zr metal center, and this step exergonic provides intermediate **1c**. The overall Gibbs barrier to **$TS_{1a\text{-}1b}$** from the precatalyst is 27.0 kcal/mol (enthalpy barrier is 24.1 kcal/mol). Under some experimental conditions it was observed that **1c** can react to form a homodinuclear complex using the Zr Cp group as a hydrogen source to form H_2. Consistent with this observation, we calculated the energy for this process to be exergonic by 11.6 kcal/mol (see SI). Also, our calculated structure shows bridged hydrides between the Zr and Ru metal centers, and this is consistent with the x-ray structure reported and is different than the **1c** structure where the lowest energy structure does not have bridging, although the Ru–H distance is shorter than the Zr–H distance.

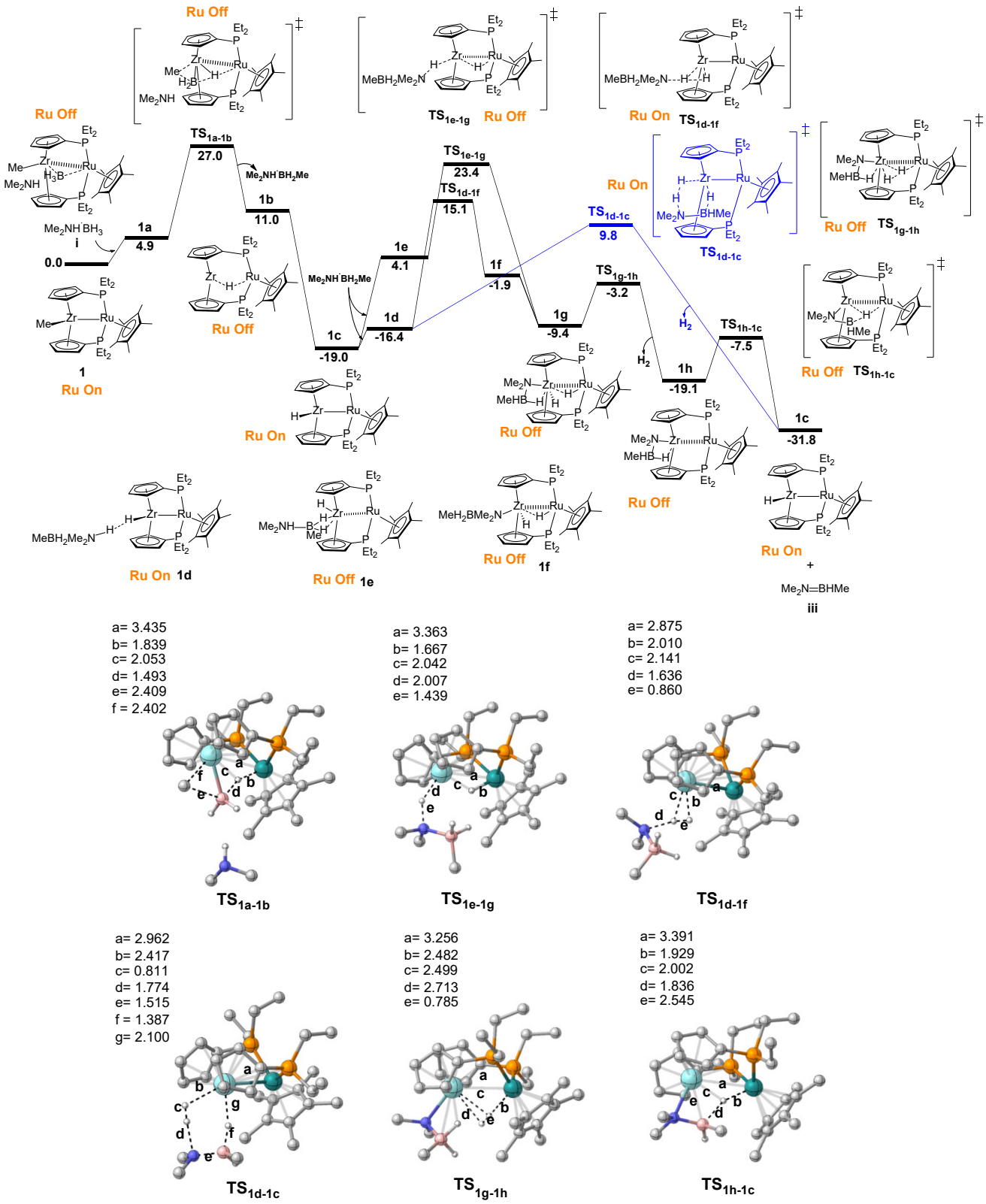

Figure 2. Top: Gibbs reaction coordinate energy profile for **1** to **1c** using Me_2NH-BH_2Me. Bottom: Optimized transition state structures for amine-borane dehydrogenation using heterobimetallic Zr-

Ru complex. Color coding: gray, carbon; blue, nitrogen; pink, boron; orange, phosphorus; teal, ruthenium; aqua, zirconium; white, hydrogen. All the C–H hydrogen atoms have been omitted.

$TS_{1a\text{-}1b}$ is unique for several reasons. First, dimethylamine is fully dislodged from the boron. This was unexpected because mechanisms previously proposed for catalytic amine borane dehydrogenation keep the B–N bond intact throughout the entire catalytic cycles. As a comparison, the enthalpy and Gibbs energy is 38.7 and 25.6 kcal/mol for **i** to separate to dimethylamine and borane not in proximity to the Zr-Ru complex. Dissociation of dimethylamine **1a** and remaining in the vicinity of the complex requires -5.7 kcal/mol. Second, this transition state showcases the ligand like donation of the Ru metal center towards the Zr metal center (see Scheme 1c for conceptual depiction). As required by a traditional σ-bond metathesis mechanism for a Zr metal center, there is a need for a vacant coordination site during the bond exchange process. This can either occur through cyclopentadienyl ligand conversion from η^5 to η^3 coordination or dissociation of the Ru metal center. For **$TS_{1a\text{-}1b}$** the vacant coordination site is achieved by significant elongation of the Zr−Ru distance to 3.44 Å from 2.80 Å in **1**. This means that Ru metal center provides an on-demand electron reservoir like a ligand and that during this transition state the Ru absorbs a significant portion of the shared electrons creating the nearly unoccupied orbital necessary for σ-bond metathesis. Also, after the transition state the Zr−Ru interaction is fully reformed in **1c**, and this highlights the on-demand nature of this interaction. Third, while the IRC connects **$TS_{1a\text{-}1b}$** to **1c** that has a fully intact Zr–H bond, in the transition state the hydrogen involved in metathesis has a shorter Ru–H (1.84 Å) distance than the Zr–H distance (2.05 Å). Therefore, due to the presence of the Ru and its d electrons this σ-bond metathesis involves some oxidative character of the Ru metal center. In the past there have been many reports of σ-bond metathesis transition states with metal centers that provide metal-hydride bonding and some oxidative character. However, these have always been by mononuclear complexes we a non-d^0 metal center. In this case Zr is a d^0 metal and cannot be oxidized. Therefore, the Ru metal center oxidatively assists this σ-bond metathesis reaction step but does not form a Ru–H bond. This means the Ru center can not only provide a continuum of on/off coordination to Zr but it can also participate in interactions facilitating bonding changes.

The formation of methylborane by **$TS_{1a\text{-}1b}$** can then lead to its combination with dimethylamine to generate $Me_2NH{\cdot}BH_2Me$ that can continue to react with intermediate **1c** to generate H_2 and $Me_2N{\cdot}BHMe$ (**iii**). We identified three major routes for this conversion. Alternative transition states/pathways are outlined in the SI. In the first pathway through **$TS_{1e\text{-}1g}$** the N−H activation occurs only at the Zr metal center without the involvement of the hydride and without reforming the Zr−Ru interaction. This transition state also features breaking the N−H bond but with no interaction between the Zr and the nitrogen, however, after the transition state the Zr−N bond is formed and leads to intermediate **1g**. From **1g** formation of H_2 and **iii** can occur through low barriers for formal reductive elimination (**$TS_{1g\text{-}1h}$**) and B−H bond *β*-hydride elimination (**$TS_{1h\text{-}1c}$**). Interestingly, in both of these transition states the Zr−Ru bond is broken.

In contrast to the first pathway with **$TS_{1e\text{-}1g}$** where the Zr−Ru bonding is disrupted, the second and third pathways that we considered have intact Zr−Ru bonding. The second pathway involves N−H activation using the Zr−H bond through **$TS_{1d\text{-}1f}$**. In this transition state the Zr−H directly reacts with the N−H bond to form dihydrogen. The structure is akin to a hydride protonation transition state that would normally evolve to form a coordinated dihydrogen. However, IRC and geometry optimization calculations from **$TS_{1d\text{-}1f}$** did not reveal such a dihydrogen coordinated complex. Instead, it appears that **$TS_{1d\text{-}1f}$** leads directly to structure **1f** with

a Zr−H bond and a bridged hydrogen no intervening potential-energy surface intermediate and then to **1g**. Likely **TS$_{1e-1g}$** is a transition state for a two-stage reaction where the first stage involves Zr−H protonation that generates H_2 and a corresponding Zr cation and nitrogen anion followed by a second stage for collapse of the ion pair that also triggers cleavage of the newly formed H−H bond and cleavage of the Zr−Ru bond generating a Ru hydride in **1g**.

The third major pathway we examined for N−H activation is through **TS$_{1d-1c}$**. This reaction pathway and transition state features a single reaction step where dihydrogen and **iii** are formed along with the Zr–H bond being regenerated. The bonding changes in this transition state are mainly facilitated by the Zr metal center and are reminiscent of Paul and Musgrave's transition state for the Ir pincer catalyst.[46] Therefore, it is perhaps surprising that **TS$_{1d-1c}$** where the bonding changes mainly occur on a single metal provides the lower energy pathway for dehydrogenation. Analysis of the transition-state energies for these three reaction pathways revealed that **TS$_{1d-1c}$** has a 13.6 kcal/mol lower barrier than **TS$_{1e-1g}$** and 5.3 kcal/mol lower barrier than **TS$_{1d-1f}$**. While **TS$_{1d-1c}$** is formally labeled as having an on Zr–Ru bond it is important to note that the metal-metal distance increases by nearly 0.2 Å in this transition state compared to the ground state. This highlights the on-demand donation flexibility of the metal-metal interaction that is akin to metal-ligand donation flexibility in mononuclear catalysts.

After one equivalent of $Me_2NH{\cdot}BH_2Me$ is converted to $Me_2N{\cdot}BHMe$ (**iii**) and H_2 intermediate **1c** can then induce the sustained catalytic cycle for the conversion of **i** to $Me_2N{=}BH_2$. Figure 3 outlines this catalytic cycle reaction coordinate energy landscape, and because the substrate differs by only a methyl group the landscape is similar to that presented in Figure 2. The landscape in Figure 3 can be used to evaluate the rate controlling intermediate and transition state for dehydrogenation. From an energy span type analysis, the resting state is likely the Zr−H intermediate and **TS$_{1i-1c}$** is the catalytic rate controlling transition state with a barrier of 27.8 kcal/mol.

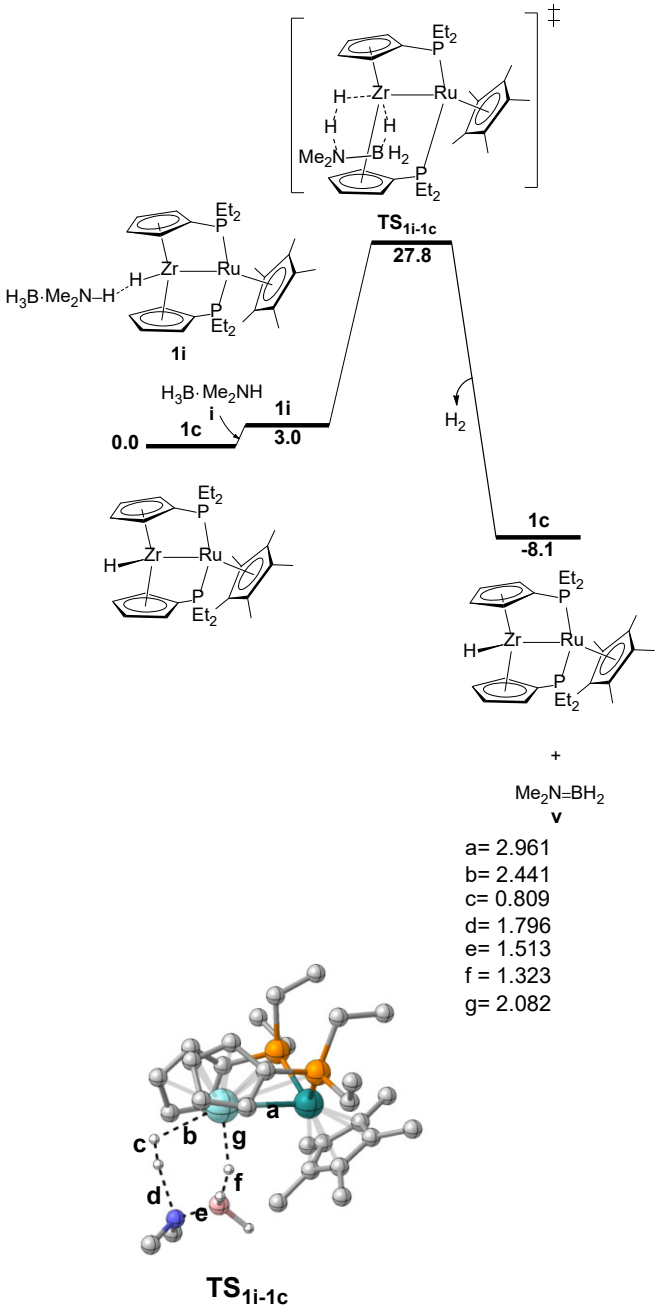

Figure 3. Top: Gibbs energy profile for **1c** to **1c** using Me_2NH-BH_3 . Bottom: Optimized transition state structures for amine-borane dehydrogenation using heterobimetallic Zr-Ru complex. Color coding: gray, carbon; blue, nitrogen; pink, boron; orange, phosphorus; teal, ruthenium; aqua, zirconium; white, hydrogen. All the C−H hydrogen atoms have been omitted.

A major impetus for our evaluation of dehydrogenation by the Zr-Ru complex was the identification of the unique features the dinuclear catalyst offers. As discussed earlier, and shown in Figures 2 and 3, there is clearly structural and mechanistic implications where the Ru metal center can play an on-demand electron donation role and participate in some direct bonding. We also wanted to evaluate the relative energies of the dinuclear catalytic cycle versus reasonable

models for mononuclear catalysts, and this provides another viewpoint of the importance of the on-demand Ru interaction with Zr.

Therefore, we first examined the mononuclear Ru complex **3** and then the mononuclear Zr complex **2**. Complex **3** was chosen because Nishibayashi experimentally tested this complex, and it showed only a small amount of dehydrogenation conversion. Complex **2** was selected because it provides a Zr metal center with two cyclopentadienyl ligands and the Ru center is replaced by a chloride ligand, and this provides a simple and straightforward mononuclear model that has significant relationship to the Zr-Ru heterodinuclear catalyst.

Figure 4 shows the Gibbs free energy landscape for amine-borane dehydrogenation with the Ru complex **3**. The coordination of $Me_2NH{\cdot}BH_3$ **i** to **3** is endergonic by 4.3 kcal/mol and the hydride abstraction transition state (**TS$_{3a\text{-}3b}$**) generates intermediate **3b** that is a σ-complex. In a subsequent step dihydrogen is lost. The barrier for dihydrogen formation with this Ru catalyst has a barrier of about 30 kcal/mol and this is in the vicinity of the barrier for the Zr-Ru catalyst generating dihydrogen. We were at first surprised that there are similar barriers for generating dihydrogen with **3** and Zr-Ru since they have fundamentally different transition-state structures and experimentally **3** is much less reactive. This prompted us to examine the remainder of the catalytic cycle where **3c** is converted back to **3** and **v** is formed. From **3b** we located the *β*-hydride elimination transition state, **TS$_{3c\text{-}3}$**. This revealed that the overall barrier for this elimination transition state added to the barrier for dihydrogen formation is 48.3 kcal/mol which is >15 kcal/mol higher that the overall barrier for the Zr-Ru complex. The single reaction step (**TS$_{3a\text{-}3}$**) was also calculated with **3** and that barrier is even higher than **TS$_{3c\text{-}3}$** about ~11 kcal/mol. Overall, this shows that for the mononuclear Ru complex the B−H activation reaction step is rate limiting, and this is different than the Ru−Zr catalysis.

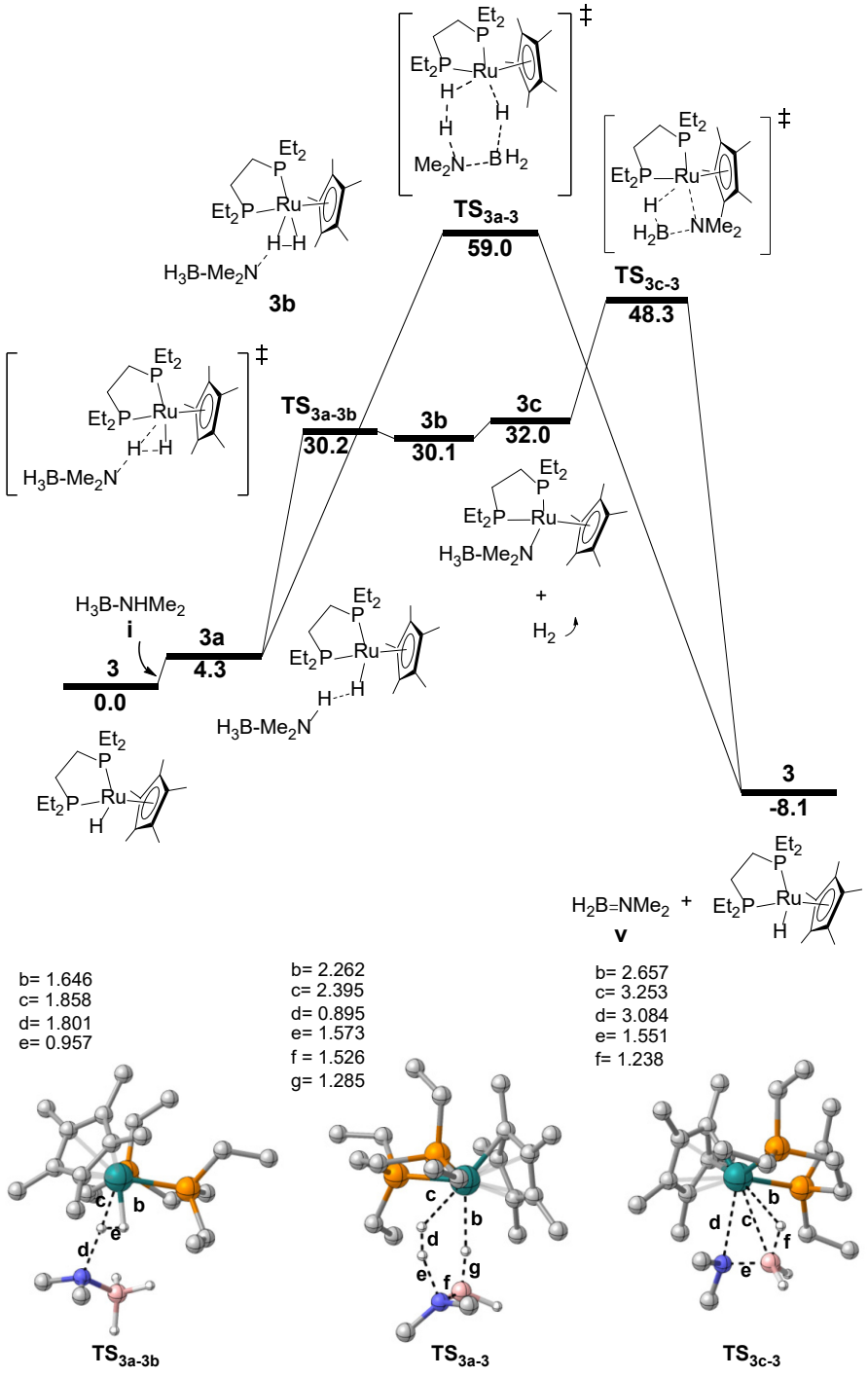

Figure 4. Top: Gibbs energy profile for amine-borane dehydrogenation using mononuclear Ru-complex. Bottom: optimized transition state structures for amine-borane dehydrogenation using mononuclear Ru-complex. Color coding: gray, carbon; blue, nitrogen; pink, boron; orange, phosphorus; teal, ruthenium; aqua, zirconium; white, hydrogen. All the C−H hydrogen atoms have been omitted.

After establishing why the reaction with the mononuclear Ru complex **3** is less reactive than the reaction with the Zr-Ru complex we then examined the transition states and intermediates for the reasonable but hypothetical mononuclear Zr complex **2**. Figure 5 shows the Gibbs free energy profile for amine-borane dehydrogenation with complex **2**. While there is the possibility of different transition states and pathways for a mononuclear Zr complex versus the Zr-Ru complex, we only directly compared the transition state for the lowest energy pathway identified from Figure 2, which is **TS$_{1i\text{-}1c}$**. This transition state is a single reaction step where dihydrogen and the amine borane is formed along with the Zr–H bond being regenerated. Figure 5 shows this transition state for the mononuclear model with **TS$_{2a\text{-}2b}$**. We initially suspected that the change from heterodinuclear to a mononuclear Zr complex would lead to a very high barrier for this amine borane dihydrogen reaction step. However, and surprisingly, this model complex showed a Gibbs energy barrier of 27.1 kcal/mol, which is a barrier very similar to the Zr-Ru complex. The subsequent β-hydride elimination reaction step that converts **2b** back to **2** has a small barrier of only 12.8 kcal/mol. Overall, this suggests that while indeed the heterodinuclear Zr-Ru has a reactivity advantage versus a Ru mononuclear complex there is no significant reactivity advantage over mononuclear Zr complexes, which were not tested by Nishibayashi. However, this does highlight two possible advantages of the Zr-Ru catalysis, which are likely catalyst stability as well as precatalyst to catalyst activation.

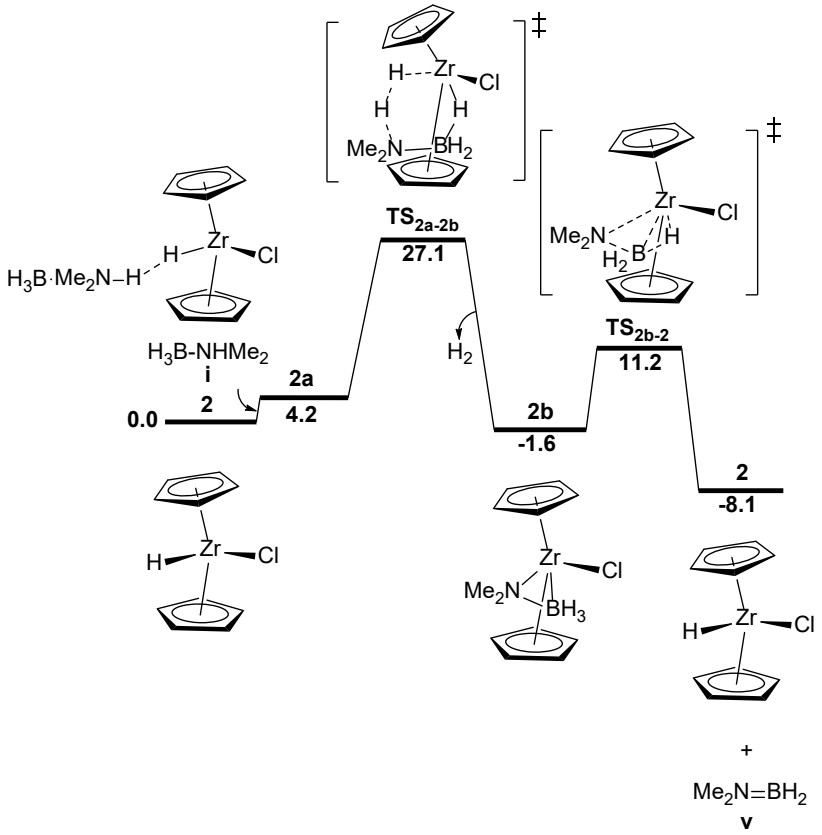

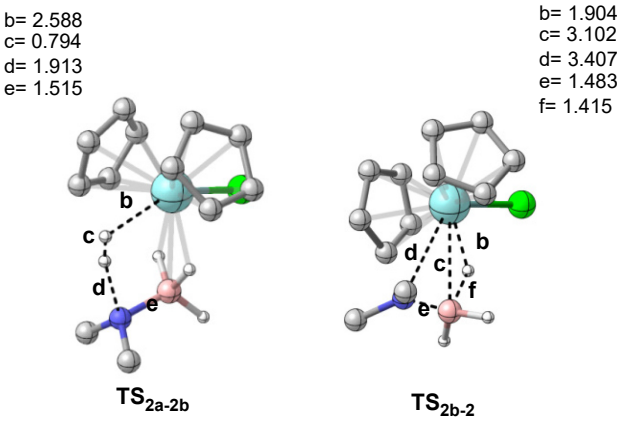

Figure 5. Top: Gibbs energy profile for amine-borane dehydrogenation using mononuclear Zr-complex. Bottom: optimized transition state structures for amine-borane dehydrogenation using mononuclear Zr-complex. Color coding: gray, carbon; blue, nitrogen; pink, boron; orange, phosphorus; teal, ruthenium; aqua, zirconium; white, hydrogen. All the C−H hydrogen atoms have been omitted.

Conclusions

Our DFT calculations revealed the cooperative metal-metal bonding in the heterodinuclear Zr-Ru catalyzed amine-borane dehydrogenation. For both N–H and B–H activation reaction steps the bonding changes is dominated by the Zr metal center. However, the Ru plays a key on-demand donation role. Comparison of mechanisms and barriers for mononuclear Zr and Ru complexes highlighted that mononuclear Ru catalysts, at least the analogous to the Zr-Ru complex and tested by Nishibayashi indeed is kinetically slow. However, a model mononuclear Zr complex showed a similar amine borane dehydrogenation barrier compared to the Zr-Ru complex. This suggests that the major advantage of the Zr-Ru complex might not be in reactivity but rather in precatalyst activation and catalyst stability.

Computational Details

Gaussian 16[71] was used for the optimization of intermediate and transition-state structures using the default ultrafine integration grid combined with the B3LYP-D3(BJ) hybrid density functional and def2-SVP basis set.[72,73,74,75] All of the stationary points were characterized either as a minimum or a first-order saddle point using vibrational frequency analysis. For transition-state structures, intrinsic reaction coordinate calculations were also carried out to verify proposed potential-energy surface connections.[76] During both optimization and single point calculations solvent effects were included using the conductor-like polarizable continuum model (CPCM) method for toluene.[77] Single-point energies were calculated using double hybrid functional B2PLYP-D3(BJ)/def2-TZVPP in ORCA,[78] and reported energies refer to B2PLYP-D3(BJ)/def2-TZVPP//B3LYP-D3(BJ)/def2-SVP.

Supporting Information

Additional reaction pathway details and xyz coordinates and absolute energies of optimized structures.

Corresponding Author Information

***Daniel H. Ess** – *Department of Chemistry and Biochemistry, Brigham Young University, Provo, Utah 84604, United States*; Email: dhe@byu.edu

Acknowledgments
The authors thank Brigham Young University and the Fulton Supercomputing Lab for computational resources. This work was supported by the US National Science Foundation with award CHE-2153215. We thank James Coombs for help with preliminary calculations.

References

1. Sinfelt, J. H. Bimetallic Catalysts: Discoveries, Concepts and Applications; John Wiley and Sons: New York, **1983**, XI + 164 pp.
2. Bullock, R. M.; Casey, C. P. Heterobimetallic Compounds Linked by Heterodifunctional Ligands. *Acc. Chem. Res.* **1987**, *20*, 167−173.
3. Stephan, D. W. Early-late Heterobimetallics. *Coord. Chem. Rev.* **1989**, *95*, 41−107.
4. Beuken, E. K. van den; Feringa, B. L. Bimetallic Catalysis by Late Transition Metal Complexes. *Tetrahedron* **1998**, *54*, 12985−13011.
5. Wheatley, N.; Kalck, P. Structure and Reactivity of Early-Late Heterobimetallic Complexes. *Chem. Rev.* **1999**, *99*, 3379−3419.
6. Gade, L. H. Highly Polar Metal-Metal Bonds in "Early-Late" Heterobimetallic Complexes. *Angew. Chem. Int. Ed.* **2000**, *39*, 2658−2678.
7. Thomas, C. M. Metal-metal Multiple Bonds in Early/Late Heterobimetallic Complexes: Applications Toward Small Molecule Activation and Catalysis. Comments Inorg. Chem. **2011**, 32, 14−38.
8. Cooper, B. G.; Napoline, J. W.; Thomas, C. M. Catalytic Applications of Early/Late Heterobimetallic Complexes. *Catal. Rev.* **2012**, 54, 1−40.
9. Mankad, N. P. Selectivity Effects in Bimetallic Catalysis. *Chem. Eur. J.* **2016**, *22*, 5822-5829.
10. Powers, D. C.; Ritter, T. Bimetallic Redox Synergy in Oxidative Palladium Catalysis. *Acc. Chem. Res.* **2012**, *45*, 840−850.
11. Berry, J. F. Metal-Metal Multiple Bonded Intermediates in Catalysis. *J. Chem. Sci.* **2015**, *127*, 209−214.
12. Buchwalter, P.; Rose, J.; Braunstein, P. Multimetallic Catalysis Based on Heterometallic Complexes and Clusters. *Chem. Rev.* **2015**, *115*, 28−126.
13. Ed. Kalck, P.; Homo- and Heterobimetallic Complexes in Catalysis: Cooperative Catalysis Topics in Organometallic Chemistry, Vol. 59, **2016**, Springer.
14. Powers, I. G.; Uyeda, C. Metal-Metal Bonds in Catalysis. *ACS Catal.* **2017**, 7, 936−958.
15. Pye, D. R.; Mankad, N. P. Bimetallic catalysis for C-C and C-X coupling reactions. *Chem. Sci.* **2017**, *8*, 1705−1718.
16. Man, M. L.; Lam, K. C.; Sit, W. N.; Ng, S. M.; Zhou, Z.; Lin, Z.; Lau, C. P. Synthesis of heterobimetallic Ru-Mn complexes and the coupling reactions of epoxides with carbon dioxide catalyzed by these complexes. *Chem. - Eur. J.* **2006**, *12*, 1004−1015.
17. Napoline, J. W.; Bezpalko, M. W.; Foxman, B. M.; Thomas, C. M. N–H activation of hydrazines by a heterobimetallic Zr–Co complex: promotion of one-electron chemistry at Zr. *Chemical Communications* **2013**, *49*, 4388-4390.
18. Krogman, J. P.; Foxman, B. M.; Thomas, C. M. Activation of CO2 by a Heterobimetallic Zr/Co Complex. *J. Am. Chem. Soc.* **2011**, *133*, 14582−14585.

19. Krogman, J. P.; Bezpalko, M. W.; Foxman, B. M.; Thomas, C. M. Synthesis, Structure, and Reactivity of an Anionic Zr–Oxo Relevant to CO2 Reduction by a Zr/Co Heterobimetallic Complex. *Inorg. Chem.* **2013**, *52*, 3022−3031.
20. Marquard, S. L.; Bezpalko, M. W.; Foxman, B. M.; Thomas, C. M. Interaction and Activation of Carbon–Heteroatom π Bonds with a Zr/Co Heterobimetallic Complex. *Organometallics* **2014**, *33*, 2071−2079.
21. Seki, R.; Hara, N.; Saito, T.; Nakao, Y. Selective C−O Bond Reduction and Borylation of Aryl Ethers Catalyzed by a Rhodium−Aluminum Heterobimetallic Complex. *J. Am. Chem. Soc.* **2021**, *143*, 6388−6394.
22. Hara, N.; Saito, T.; Semba, K.; Kuriakose, N.; Zheng, H.; Sakaki, S.; Nakao, Y. Rhodium Complexes Bearing PAlP Pincer Ligands. *J. Am. Chem. Soc.* **2018**, *140*, 7070−7073.
23. Fujii, I.; Semba, K.; Li, Q.-Z.; Sakaki, S.; Nakao, Y. Magnesiation of Aryl Fluorides Catalyzed by a Rhodium−Aluminum Complex. *J. Am. Chem. Soc.* **2020**, *142*, 11647−11652.
24. Takaya, J.; Iwasawa, N. Synthesis, Structure, and Catalysis of Palladium Complexes Bearing a Group 13 Metalloligand: Remarkable Effect of an Aluminum-Metalloligand in Hydrosilylation of CO2. *J. Am. Chem. Soc.* **2017**, *139*, 6074−6077.
25. Staubitz, A.; Robertson, A. P. M.; Sloan, M. E.; Manners, I. Amine− and Phosphine−Borane Adducts: New Interest in Old Molecules. *Chem. Rev.* **2010**, *110*, 4023−4078.
26. Hamilton, C. W.; Baker, R. T.; Staubitz, A.; Manners, I. B–N compounds for chemical hydrogen storage. *Chem. Soc. Rev.* **2009**, *38*, 279−293.
27. Vance, J. R.; Schäfer, A.; Robertson, A. P. M.; Lee, K.; Turner, J.; Whittell, G. R.; Manners, I. Iron-Catalyzed Dehydrocoupling/Dehydrogenation of Amine–Boranes. *J. Am. Chem. Soc.* **2014**, *136*, 3048−3064.
28. Staubitz, A.; Sloan, M. E.; Robertson, A. P. M.; Friedrich, A.; Schneider, S.; Gates, P. J.; Schmedt auf der Günne, J.; Manners, I. Catalytic Dehydrocoupling/Dehydrogenation of N-Methylamine-Borane and Ammonia-Borane: Synthesis and Characterization of High Molecular Weight Polyaminoboranes. *J. Am. Chem. Soc.* **2010**, *132*, 13332−13345.
29. Sloan, M. E.; Staubitz, A.; Clark, T. J.; Russell, C. A.; Lloyd-Jones, G. C.; Manners, I. Homogeneous Catalytic Dehydrocoupling/Dehydrogenation of Amine−Borane Adducts by Early Transition Metal, Group 4 Metallocene Complexes. *J. Am. Chem. Soc.* **2010**, *132*, 3831−3841.
30. Robertson, A. P. M.; Suter, R.; Chabanne, L.; Whittell, G. R.; Manners, I. Heterogeneous Dehydrocoupling of Amine–Borane Adducts by Skeletal Nickel Catalysts. *Inorg. Chem.* **2011**, *50*, 12680−12691.
31. Robertson, A. P. M.; Haddow, M. F.; Manners, I. Synthesis and the Thermal and Catalytic Dehydrogenation Reactions of Amine-Thioboranes. *Inorg. Chem***. 2012**, *51*, 8254−8264.
32. Metters, O. J.; Flynn, S. R.; Dowds, C. K.; Sparkes, H. A.; Manners, I.; Wass, D. F. Catalytic Dehydrocoupling of Amine–Boranes using Cationic Zirconium(IV)–Phosphine Frustrated Lewis Pairs. *ACS Catal.* **2016**, *6*, 6601−6611.
33. LaPierre, E. A.; Patrick, B. O.; Manners, I. Trivalent Titanocene Alkyls and Hydrides as Well-Defined, Highly Active, and Broad Scope Precatalysts for Dehydropolymerization of Amine-Boranes. *J. Am. Chem. Soc.* **2019**, *141*, 20009−20015.
34. Johnson, H. C.; Leitao, E. M.; Whittell, G. R.; Manners, I.; Lloyd-Jones, G. C.; Weller, A. S. Mechanistic Studies of the Dehydrocoupling and Dehydropolymerization of Amine–Boranes Using a [Rh(Xantphos)]+ Catalyst. *J. Am. Chem. Soc.* **2014**, *136*, 9078−9093.

35. Lin, T.-P.; Peters, J. C. Boryl-Mediated Reversible H2 Activation at Cobalt: Catalytic Hydrogenation, Dehydrogenation, and Transfer Hydrogenation. *J. Am. Chem. Soc.* **2013**, *135*, 15310−15313.
36. Miyazaki, T.; Tanabe, Y.; Yuki, M.; Miyake, Y.; Nishibayashi, Y. Synthesis of Group IV (Zr, Hf)−Group VIII (Fe, Ru) Heterobimetallic Complexes Bearing Metallocenyl Diphosphine Moieties and Their Application to Catalytic Dehydrogenation of Amine−Boranes. *Organometallics* **2011**, *30*, 2394−2404.
37. Stephens, F. H.; Pons, V.; Tom Baker, R. Ammonia–borane: the hydrogen source par excellence? *Dalton Trans.* **2007**, 2613−2626.
38. Smythe, N. C.; Gordon, J. C. Ammonia Borane as a Hydrogen Carrier: Dehydrogenation and Regeneration. *Eur. J. Inorg. Chem.* **2010**, *2010*, 509−521.
39. Sutton, A. D.; Burrell, A. K.; Dixon, D. A.; Garner, E. B.; Gordon, J. C.; Nakagawa, T.; Ott, K. C.; Robinson, J. P.; Vasiliu, M. Regeneration of Ammonia Borane Spent Fuel by Direct Reaction with Hydrazine and Liquid Ammonia. *Science* **2011**, *331*, 1426−1429.
40. Davis, B. L.; Dixon, D. A.; Garner, E. B.; Gordon, J. C.; Matus, M. H.; Scott, B.; Stephens, F. H. Efficient Regeneration of Partially Spent Ammonia Borane Fuel. *Angew. Chem. Int. Ed.* **2009**, *48*, 6812−6816.
41. Reller, C.; Mertens, F. O. R. L. A Self-Contained Regeneration Scheme for Spent Ammonia Borane Based on the Catalytic Hydrodechlorination of BCl3. *Angew. Chem. Int. Ed.* **2012**, *51*, 11731−11735.
42. Whittell, G. R.; Manners, I. Advances with Ammonia-Borane: Improved Recycling and Use as a Precursor to Atomically Thin BN Films. *Angew. Chem. Int. Ed.* **2011**, *50*, 10288−10289.
43. Clark, T. J.; Lee, K.; Manners, I. Transition-Metal-Catalyzed Dehydrocoupling: A Convenient Route to Bonds between Main-Group Elements. *Chem. - Eur. J.* **2006**, *12*, 8634−8648.
44. Bhunya, S.; Malakar, T.; Ganguly, G.; Paul, A. Combining Protons and Hydrides by Homogeneous Catalysis for Controlling the Release of Hydrogen from Ammonia-Borane: Present Status and Challenges. *ACS Catal.* **2016**, *6*, 7907-7934.
45. Pai, S. J.; Han, S. S. S_E2 reaction in noncarbon system: Metal-halide catalysis for dehydrogenation of ammonia borane. *Proc. Nat. Acad. Sci.* **2017**, *114*, 13625−13630.
46. Paul, A.; Musgrave, C. B. Catalyzed Dehydrogenation of Ammonia-Borane by Iridium Dihydrogen Pinacer Complex Differs from Ethane Dehydrogenation. *Angew. Chem. Int. Ed.* **2007**, *46*, 8153−8156.
47. Ghatak, K.; Vanka, K. A computational investigation of the role of the iridium dihydrogen pincer complex in the formation for the cyclic pentamer $(NH_2BH_2)_5$. *Computational and Theoretical Chemistry* **2012**, *992*, 18−29.
48. Ai, D-X.; Qi, Z-H.; Ruan, G-Y.; Liu, W.; Wang, Y. DFT studies of dehydrogenation of ammonia-borane catalyzed by $[Ir(I^tBu')_2]^+$: A proton transfer mechanism. *Computational and Theoretical Chemistry* **2014**, *1048*, 1−6.
49. Titova, E. M.; Osipova, E. S.; Pavlov, A. A.; Filippov, O. A.; Safronov, S. V.; Shubina, E. S.; Belkova, N. V. Mechanism of Dimethylamine−Borane Dehydrogenation Catalyzed by an Iridium(III) PCP-Pincer Complex. *ACS Catal.* **2017**, *7*, 2325−2333.
50. Zhang, Y.; Zhang, Y.; Qi, Z-H.; Gao, Y.; Liu, W.; Wang, Y. Ammonia-borane dehydrogenation catalyzed by Iron pincer complexes: A concerted metal-ligand cooperation mechanism. *Int. J. of Hydrogen Energy* **2016**, *41*, 17208−17215.

51. Brodie, C. N.; Boyd, T. M.; Macgregor, S. A.; Weller, A. S. Dehydropolymerization of $H_3B{\cdot}NMeH_2$ Mediated by Cationic Iridium(III) Precatalysts Bearing κ^3-^{i}Pr-PN^{R}P Pincer Ligands (R = H, Me): An Unexpected Inner-Sphere Mechanism. *ACS Catal.* **2022**, *12*, 13050−13064.
52. Luo, Y.; Ohno, K. Computational Study of Titanocene-Catalyzed Dehydrocoupling of the Adduct $Me_2NH{\cdot}BH_3$: An Intramolecular, Stepwise Mechanism. *Organometallics* **2007**, *26*, 3597−3600.
53. Friedrich, A.; Drees, M.; Schneider, S. Ruthenium-Catalyzed Dimethylamineborane Dehydrogenation: Stepwise Metal-Centered Dehydrocyclization. *Chem. Eur. J.* **2009**, *15*, 10339−10342.
54. Esteruelas, M. A.; Nolis, P.; Oliván, M.; Oñate, E.; Vallribera, A.; Vélez, A. Ammonia Borane Dehydrogenation Promoted by a Pincer-Square-Planar Rhodium(I) Monohydride: A Stepwise Hydrogen Transfer from the Substrate to the Catalyst. *Inorg. Chem.* **2016**, *55*, 7176−7181.
55. Kawano, Y.; Uruichi, M.; Shimoi, M.; Taki, S.; Kawaguchi, T.; Kakizawa, T.; Ogino, H. Dehydrocoupling Reactions of Borane−Secondary and −Primary Amine Adducts Catalyzed by Group-6 Carbonyl Complexes: Formation of Aminoboranes and Borazines. *J. Am. Chem. Soc.* **2009**, *131*, 14946−14957.
56. Roselló-Merino, M.; López-Serrano, J.; Conejero, S. Dehydrocoupling Reactions of Dimethylamine-Borane by Pt(II) Complexes: A New Mechanism Involving Deprotonation of Boronium Cations. *J. Am. Chem. Soc.* **2013**, *135*, 10910−10913.
57. Marziale, A. N.; Friedrich, A.; Klopsch, I.; Dress, M.; Celinski, V. R.; auf der Günne, J. S.; Schneider, S. The Mechanism of Borane-Amine Dehydrocoupling with Bifunctional Ruthenium Catalysts. *J. Am. Chem. Soc.* **2013**, *135*, 13342-13355.
58. Yang, X.; Hall, M. B. The Catalytic Dehydrogenation of Ammonia-Borane Invovling an Unexpected Hydrogen Transfer to Ligated Carbene and Subsequent Carbon−Hydrogen Activation. *J. Am Chem. Soc.* **2008**, *130*, 1798−1799.
59. Yang, X.; Hall, M. B. Density functional theory study of the mechanism for $Ni(NHC)_2$ catalyzed dehydrogenation of ammonia-borane for chemical hydrogen storage. *J. Organomet. Chem.* **2009**, *694*, 2831−2838.
60. Ai, D.; Guo, Y.; Liu, W.; Wang, Y. DFT studies on catalytic dehydrogenation of ammonia borane by $Ni(NHC)_2$. *J. Phys. Org. Chem.* **2014**, *27*, 597−603.
61. Zimmerman, P. M.; Paul, A.; Musgrave, C. B. Catalytic Dehydrogenation of Ammonia Borane at Ni Monocarbene and Dicarbene Catalysts. *Inorg. Chem.* **2009**, *48*, 5418−5433.
62. Zhang, Y.; Wang, P.; Gao, Y.; Zhang, Y.; Qi, Z-H.; Liu, W.; Wang, Y. Mechanistic insights into tandem amine-borane dehydrogenation and alkene hydrogenation catalyzed by $[Pd(NHC)(PCy_3)]$. *Int. J. of Hydrogen Energy* **2018**, *43*, 2043−2049.
63. Peng, C.; Zhang, Y.; Wang, Y.; Liu, W.; Yang, Y. Theoretical exploration of the mechanisms on the iron complexes catalyzed ammonia borane dehydrogenation and polyaminoborane formation. *Int. J. of Hydrogen Energy* **2023**, *48*, 23633−23644.
64. Zimmerman, P. M.; Paul, A.; Zhang, Z.; Musgrave, C. B. The Role of Free N-Heterocyclic Carbene (NHC) in the Catalytic Dehydrogenation of Ammonia-Borane in the Nickel NHC System. *Angew. Chem. Int. Ed.* **2009**, *48*, 2201−2205.
65. Butera, V.; Russo, N.; Sicilia, E. Do Rhodium Bis(σ-amine−borane) Complexes Play a Role as Intermediates in Dehydrocoupling Reactions of Amine-Boranes?. *Chem. Eur. J.* **2011**, *17*, 14586−14592.

66. Douglas, T. M.; Chaplin, A. B.; Weller, A. S. Amine-Borane σ-Complexes of Rhodium. Relevance to the Catalytic Dehydrogenation of Amine-Boranes. *J. Am. Chem. Soc.* **2008**, *130*, 14432−14433.
67. Douglas, T. M.; Chaplin, A. B.; Weller, A. S.; Yang, X.; Hall, M. B. Monomeric and Oligomeric Amine−Borane σ-Complexes of Rhodium. Intermediates in the Catalytic Dehydrogenation of Amine−Boranes. *J. Am. Chem. Soc.* **2009**, *131*, 15440−15456.
68. Dallanegra, R.; Chaplin, A. B.; Weller, A. S. Bis(σ-amine−borane) Complexes: An Unusual Binding Mode at a Transition-Metal Center. *Angew. Chem. Int. Ed.* **2009**, *48*, 6875−6878.
69. Algarra, A. G.; Sewell, L. J.; Johnson, H. C.; Macgregor, S. A.; Weller, A. S. A combined experimental and computational study of fluxional processes in sima amine-borane complexes of rhodium and iridium. *Dalton Trans.* **2014**, *43*, 11118−11128.
70. Alcaraz, G.; Vendier, L.; Clot, E.; Sabo-Etienne, S. Ruthenium Bis(σ-B−H) Aminoborane Complexes from Dehydrogenation of Amine−Boranes: Trapping of $H_2B{-}NH_2$. *Angew. Chem. Int. Ed.* **2010**, *49*, 918−920.
71. Frisch, M. J.; Trucks, G. W.; Schlegel, H. B.; Scuseria, G. E.; Robb, M. A.; Cheeseman, J. R.; Scalmani, G.; Barone, V.; Petersson, G. A.; Nakatsuji, H.; Li, X.; Caricato, M.; Marenich, A. V.; Bloino, J.; Janesko, B. G.; Gomperts, R.; Mennucci, B.; Hratchian, H. P.; Ortiz, J. V.; Izmaylov, A. F.; Sonnenberg, J. L.; Williams-Young, D.; Ding, F.; Lipparini, F.; Egidi, F.; Goings, J.; Peng, B.; Petrone, A.; Henderson, T.; Ranasinghe, D.; Zakrzewski, V. G.; Gao, J.; Rega, N.; Zheng, G.; Liang, W.; Hada, M.; Ehara, M.; Toyota, K.; Fukuda, R.; Hasegawa, J.; Ishida, M.; Nakajima, T.; Honda, Y.; Kitao, O.; Nakai, H.; Vreven, T.; Throssell, K.; Montgomery, Jr., J. A.; Peralta, J. E.; Ogliaro, F.; Bearpark, M. J.; Heyd, J. J.; Brothers, E. N.; Kudin, K. N.; Staroverov, V. N.; Keith, T. A.; Kobayashi, R.; Normand, J.; Raghavachari, K.; Rendell, A. P.; Burant, J. C.; Iyengar, S. S.; Tomasi, J.; Cossi, M.; Millam, J. M.; Klene, M.; Adamo, C.; Cammi, R.; Ochterski, J. W.; Martin, R. L.; Morokuma, K.; Farkas, O.; Foresman, J. B.; Fox, D. J. Gaussian 16, revision B.01; Gaussian, Inc.: Wallingford CT, **2016**.
72. Becke, A. D. Density-functional thermochemistry. III. The role of exact exchange. *J. Chem. Phys.* **1993**, *98*, 5648−5652.
73. Grimme, S.; Antony, J.; Ehrlich, S.; Krieg, H. A consistent and accurate ab initio parametrization of density functional dispersion correction (DFT-D) for the 94 elements H-Pu. *J. Chem. Phys.***2010**, *132*, 154104.
74. Grimme, S.; Ehrlich, S.; Goerigk, L. Effect of the damping function in dispersion corrected density functional theory. *J. Comput. Chem.* **2011**, *32*, 1456−1465.
75. Weigend, F.; Ahlrichs, R. Balanced basis sets of split valence, triple zeta valence and quadruple zeta valence quality for H to Rn: Design and assessment of accuracy. *Phys. Chem. Chem. Phys.* **2005**, *7*, 3297−3305.
76. Fukui, K. The path of chemical reactions - the IRC approach. *Acc. Chem. Res.* **1981**, *14*, 363−368.
77. Tomasi, J.; Mennucci, B.; Cammi, R. Quantum Mechanical Continuum Solvation Models. *Chem. Rev.* **2005**, *105*, 2999−3094.
78. Neese, F. The ORCA program system. *WIREs Comput. Mol. Sci.* **2022**, 12, e1491.

TOC graphic

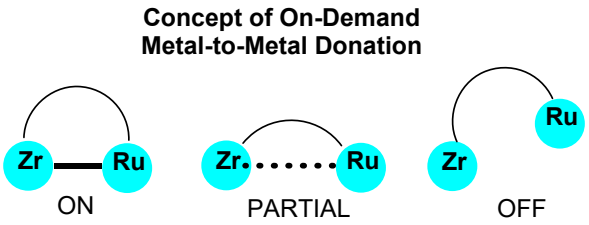
Concept of On-Demand
Metal-to-Metal Donation
Zr
Ru
ON
Zr
Ru
PARTIAL
Zr
Ru
OFF